Vrije Universiteit Brussel

VRIJE
UNIVERSITEIT
BRUSSEL

Optical-quality controllable wet-chemical doping of graphene through a uniform, transparent and low-roughness F4-TCNQ/MEK layer

Misseeuw, Lara Renée; Krajewska, Aleksandra; Pasternak, Iwona; Ciuk, Tymoteusz; Strupinski, Wlodek; Reekmans, Gunter; Adriaensens, Peter; Geldof, Davy; Blockhuys, F.; Van Vlierberghe, Sandra; Thienpont, Hugo; Dubruel, Peter; Vermeulen, Nathalie

Link to publication

CrossMark
click for updates

Optical-quality controllable wet-chemical doping of graphene through a uniform, transparent and low-roughness F4-TCNQ/MEK layer†

Lara Misseeuw,*[a] Aleksandra Krajewska,[bc] Iwona Pasternak,[c] Tymoteusz Ciuk,[c] Wlodek Strupinski,[c] Gunter Reekmans,[d] Peter Adriaensens,[d] Davy Geldof,[e] Frank Blockhuys,[e] Sandra Van Vlierberghe,[aef] Hugo Thienpont,[a] Peter Dubruel[f] and Nathalie Vermeulen[a]

Controllable chemical doping of graphene has already proven very useful for electronic applications, but when turning to optical and photonic applications, the additional requirement of having both a high transparency and a low surface roughness has, to our knowledge, not yet been fulfilled by any chemical dopant system reported so far. In this work, a new method that meets for the first time this optical-quality requirement while also providing efficient, controllable doping is presented. The method relies on F4-TCNQ dissolved in methyl ethyl ketone (MEK) yielding a uniform deposition after spin coating because of an extraordinary charge transfer interaction between the F4-TCNQ and MEK molecules. The formed F4-TCNQ/MEK layer exhibits a very high surface quality and optical transparency over the visible-infrared wavelength range between 550 and 1900 nm. By varying the dopant concentration of F4-TCNQ from 2.5 to 40 mg ml^{-1} MEK, the doping effect can be controlled between $\Delta n = +5.73 \times 10^{12}$ cm^{-2} and $+1.09 \times 10^{13}$ cm^{-2} for initially strongly p-type hydrogen-intercalated graphene grown on 6H-silicon-carbide substrates, and between $\Delta n = +5.56 \times 10^{12}$ cm^{-2} and $+1.04 \times 10^{13}$ cm^{-2} for initially weakly p-type graphene transferred on silicon samples. This is the first time that truly optical-quality chemical doping of graphene is demonstrated, and the obtained doping values exceed those reported before for F4-TCNQ-based graphene doping by as much as 50%.

1. Introduction

Graphene, a monolayer of sp^2-hybridized carbon atoms ordered in a honeycomb structure, is a most promising material with unprecedented application possibilities in the fields of, amongst others, electronics, spintronics and photonics.[1] Pristine graphene exhibits truly extraordinary characteristics such as an extremely high thermal conductivity[2] ($K = 5.30 \times 10^3$ W mK^{-1} at room temperature), the ability to sustain a significant electrical current density[3] ($J = 10^8$ A cm^{-2}), a high electron mobility at room temperature[4] ($\mu = 2 \times 10^5$ cm^2 V^{-1} s^{-1}), an exceptional intrinsic strength and elasticity[5] ($\sigma_{\text{int}} = 130$ GPa and $E = 1$ TPa, respectively) and an unusually high optical absorption of 2.3% per layer.[1,6] What makes graphene even more interesting is that its electronic and optical properties can be tuned by shifting its Fermi level. Whereas pristine graphene acts like a zero-bandgap semiconductor with its Fermi level positioned at the Dirac point,[7] the position of the Fermi level can be adjusted either by applying an electrical field with a gate voltage (electrical doping)[8] or by chemical doping.[9] The latter can be roughly subdivided in substitutional doping and surface transfer doping. When a carbon atom in the graphene layer is replaced by an atom with a different number of valence electrons,[10] like boron[11] or nitrogen,[12] the sp^2-hybridization of carbon atoms will be disrupted and graphene is exposed to substitutional doping. When surface transfer doping is applied, a dopant molecule is adsorbed on the surface and causes an electron exchange between graphene and the dopant molecule.[9] Both doping mechanisms can lead to a shift of the Fermi level above or below the Dirac point, called n-type doping with an

[a]*Brussels Photonics Team (B-PHOT), Dept. of Applied Physics and Photonics (IR-TONA), Vrije Universiteit Brussel, Pleinlaan 2, B-1050 Brussels, Belgium. E-mail: lmisseeu@b-phot.org*

[b]*Institute of Optoelectronics, Military University of Technology, Gen. S. Kaliskiego 2, 00-908 Warsaw, Poland*

[c]*Institute of Electronic Materials Technology, Wolczynska 133, 01-919 Warsaw, Poland*

[d]*Applied and Analytical Chemistry, Institute for Materials Research (IMO), Hasselt University, Agoralaan 1-Building D, B-3590 Diepenbeek, Belgium*

[e]*Department of Chemistry, University of Antwerp, Groenborgerlaan 171, B-2020 Antwerp, Belgium*

[f]*Polymer Chemistry & Biomaterials Research Group, Ghent University, Krijgslaan 281 (S4 Bis), B-9000 Ghent, Belgium*

† Electronic supplementary information (ESI) available: Experimental methods. ^{13}C-NMR spectra and detailed description of F4-TCNQ dopant solutions. Tables with electrical parameters of graphene before and after doping with an F4-TCNQ/MEK layer. See DOI: 10.1039/c6ra24057g
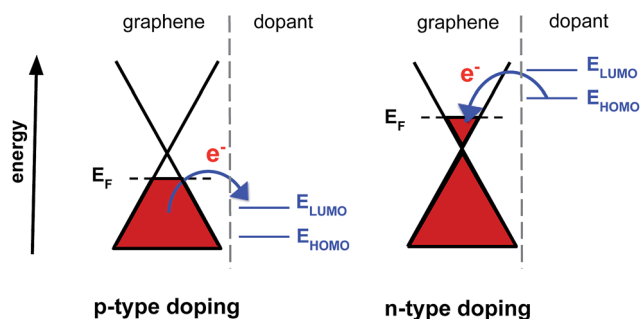
Fig. 1 Representation of p- and n-doping of graphene. Next to the graphene band diagram, the energy diagram of the electron donor or acceptor is shown with its E_{LUMO} (energy of the lowest unoccupied molecular orbital) and E_{HOMO} (energy of the highest occupied molecular orbital).[14]

Fig. 2 Chemical structure of 2,3,5,6-tetrafluoro-7,7,8,8-tetracyano-quinodimethane (F4-TCNQ).

excess of electrons or p-type doping with an excess of holes, respectively[13] (Fig. 1).

For electronic applications the effectiveness of a graphene doping method is expressed in terms of charge carrier concentration, mobility and sheet resistance. However, when considering the use of graphene in optical and photonic applications such as in photonic integrated circuits and nonlinear optics, also a high optical transparency and a low surface roughness of the dopant system are of crucial importance. Several research groups have already developed chemical dopant systems for graphene with an additional optical absorption of only a few percent for light passing perpendicularly through the graphene sheet, and some of them even reached real transparency in certain wavelength domains.[15–21] However, the latter either relied on a plasma treatment of the graphene effectively worsening the surface quality and hence the level of light scattering in the 2D material, or only induced a weak and non-controllable doping effect.[15,17,22,23]

Hence, a new doping method is needed that fulfills the requirement of having real transparency and a very low surface roughness to eliminate light scattering, while also establishing controllable and efficient doping. We here present such a method, where the active dopant compound is 2,3,5,6-tetrafluoro-7,7,8,8-tetracyanoquinodimethane (F4-TCNQ), a well-known organic electron acceptor commercially available in powder form. F4-TCNQ is frequently used for surface transfer doping of different types of material systems and devices, from OLEDs[24] (organic light-emitting diodes) and polymer transistors,[25] to diamond,[26] carbon nanotubes[27] and graphene.[13] As illustrated in Fig. 2, the dopant molecule F4-TCNQ is composed of a hexagonal ring substituted by double bonds and by strong electron-withdrawing nitrile groups and fluorine atoms.[28] The unique character of F4-TCNQ is derived partly from the polyene system with the powerful electron-withdrawing groups and partly from the planarity and high symmetry of the F4-TCNQ structure,[29] resulting in a high electron affinity[30] (E_A) of 5.2 eV. The four fluorine groups significantly increase the charge transfer in comparison with the non-fluorinated analogue TCNQ (E_A = 4.8 eV).[31] The work function of graphene was calculated[32] to be 4.5 eV, indicating that F4-TCNQ can potentially act as a powerful dopant
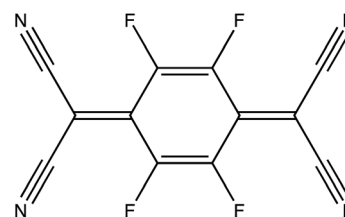
to extract electrons from graphene. We point out that, when graphene is exposed to air, some level of p-doping is already unintentionally introduced. It is therefore a natural strategy in our paper to try to further increase the p-doping by means of an electron acceptor such as F4-TCNQ. It should be noted that for optical applications it generally does not matter whether n- or p-doping is obtained, since for most light-matter interactions in graphene only the magnitude of the graphene Fermi level is important and not its sign.

The deposition of F4-TCNQ as a dopant molecule on graphene is based on the adsorption on graphene, resulting in its non-covalent functionalization[33] by dopant-substrate π–π interactions.[34] The deposition can be realized via thermal evaporation[35–37] or via wet chemistry, i.e. via a solvent-assisted method. The latter method is more advantageous in terms of practical applicability and technological relevance. Several solvents have already been employed for wet-chemical F4-TCNQ doping of polymers and carbon nanotubes including toluene,[38–40] chloroform,[38,41] tetrahydrofuran (THF),[42] isopropyl alcohol,[43] chlorobenzene, thiophene, acetonitrile and xylene.[38] For the wet-chemical doping of graphene with F4-TCNQ, only chloroform and dimethyl sulfoxide (DMSO) have been tested so far (see the work of Coletti et al.).[35] Nevertheless, of all these studies on solvent-assisted F4-TCNQ doping, regardless the material the doping is applied to, none of them report on a low surface roughness and a high optical transparency of the F4-TCNQ deposition, as is required for optical and photonic applications. As pointed out earlier, also when considering other chemical graphene doping methods not relying on F4-TCNQ, none of them fulfill the optical-quality requirement. Regarding the controllability and doping capacity of F4-TCNQ on graphene, only information about the doping obtained via thermal evaporation is, to our knowledge, available in literature. Coletti et al. obtained charge neutrality for initially n-doped graphene with a net increase in hole concentration of $+7.15 \times 10^{12}$ cm^{-2} after full coverage with vapor deposited F4-TCNQ molecule.[35]

In this paper, we show that by combining F4-TCNQ with a specific category of solvents, namely ketones, optical-quality chemical doping of graphene is established for the first time while also achieving a controllable and efficient doping effect. The requirement of optical-quality doping is fulfilled thanks to an extra-ordinary layer formation mechanism as a result of interacting F4-TCNQ and ketone molecules.

The paper consists of two parts. In the first part a comprehensive study is presented about the chemical and optical properties of the F4-TCNQ/ketone dopant combination: we
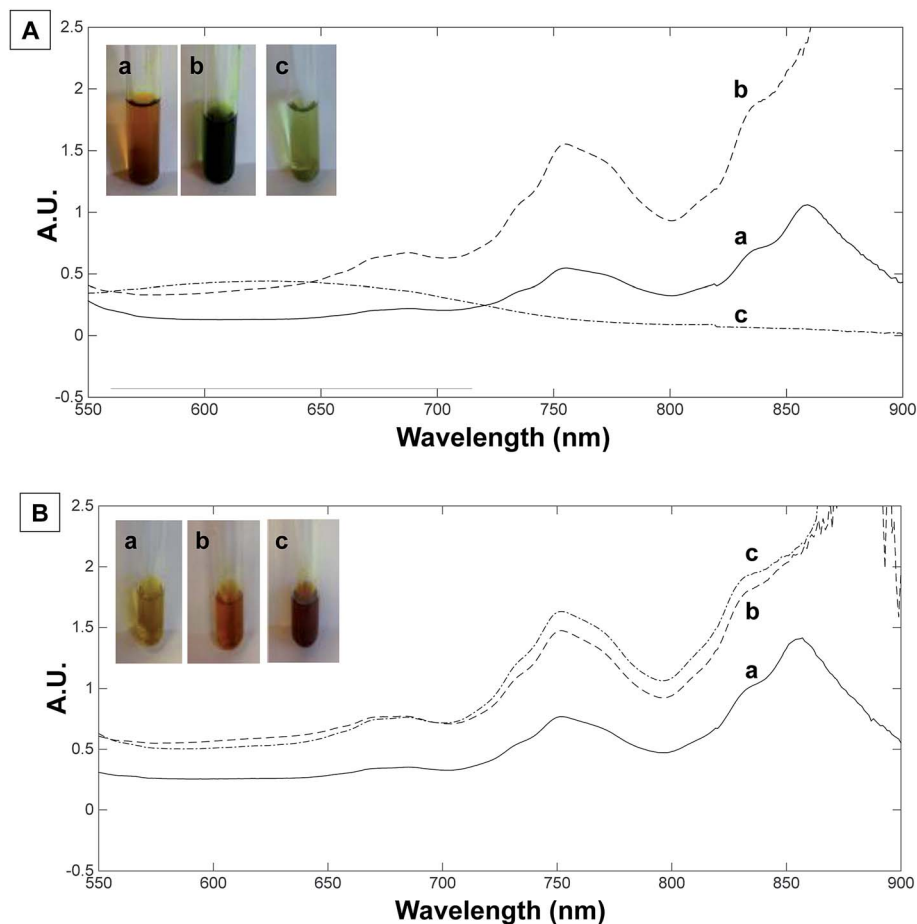
Fig. 3 UV-VIS spectra of (A) 20 mg F4-TCNQ ml^{-1} MEK solution and (B) 20 mg F4-TCNQ ml^{-1} acetonitrile solution at 3 points in time: (a) $t =$ 0 hours, (b) after heating (50 °C) and stirring for 2 hours and (c) after heating (50 °C) and stirring for 5 hours. In the inset, snapshots are shown of the color evolution of the F4-TCNQ/MEK and F4-TCNQ/acetonitrile dopant solution at the 3 points in time.

explain the hypothesis of the layer formation, and discuss the other benefits of the ketone solvents in terms of solubility and optical transparency after spin coating. The second part of the paper presents details about the actual doping effect in terms of the change of graphene's electrical properties. Here, we focus on one ketone solvent (methyl ethyl ketone or MEK) and determine the F4-TCNQ concentration dependence of the graphene doping. Finally, we address the difference between the electron withdrawing activity of F4-TCNQ incorporated in a layer with MEK and that obtained through evaporated powder deposition.

2. Results and discussion

2.1 Chemical and optical properties of F4-TCNQ/MEK solution and layer

2.1.1 Solvent dependent solubility of F4-TCNQ. First, we studied the solubility of F4-TCNQ in various solvents that had already been mentioned in literature (toluene, chloroform, DMSO, xylene, isopropyl alcohol, trichlorobenzene and acetonitrile) and additional commonly used solvents (DCM, dioxane and MEK).[37-42] We selected MEK because it is known that this ketone solvent (Fig. 4a) has a high solubility for fluorine-

containing molecules or polymers and thus also for F4-TCNQ.[44] Indeed, we found that F4-TCNQ could be readily dissolved in a concentration range between 1 and 100 mg F4-TCNQ ml^{-1} MEK (3.62 mM to 362 mM) without reaching saturation. All other solvents exhibited very poor solvation properties (*i.e.* a few mg F4-TCNQ ml^{-1} solvent), except for acetonitrile (Fig. 4g) which featured a substantial while considerably lower solubility of 60 mg F4-TCNQ ml^{-1}. Based on these solubility results, further experiments and analyses were carried out with acetonitrile and MEK.

Although the dissolution of F4-TCNQ in MEK was achieved very easily, additional stirring and heating resulted in a color change of the dopant solution in time. In order to monitor these changes, UV-VIS spectroscopy of the solutions was performed. Fig. 3A shows the absorbance at three different points in time of a 20 mg F4-TCNQ ml^{-1} MEK solution. We chose this concentration because it is the center value in the range of concentrations used for the doping experiments (see Section 2.2). Immediately after preparing the solution, the F4-TCNQ molecules were completely dissolved and the solution was yellowish orange similar to the color of F4-TCNQ in powder form (Fig. 3A(a)). The bands at 756 and 862 nm were immediately
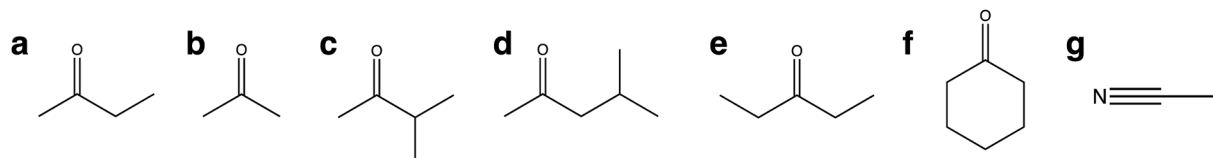
Fig. 4 The chemical structure of (a) MEK (methyl ethyl ketone or butanone) (b) acetone (c) 3-methyl-butan-2-one (d) 4-methyl-pentan-2-one (e) pentan-3-one (f) cyclohexanone and (g) acetonitrile. Solvents (a)–(f) are ketone solvents.

observed and correspond to F4-TCNQ radical anions.[45] Because F4-TCNQ has a high electron affinity of 5.2 eV,[30] it could be expected that F4-TCNQ acts as an electron acceptor and becomes negatively charged in the presence of MEK. Further stirring combined with heating in an oil bath at 50 °C for 2 hours turned the color of the dopant solution from yellowish orange to green (Fig. 3A(b)) and the F4-TCNQ anion bands reached maximal amplitude. Since TCNQ anion solutions are known to exhibit a green color,[29,46] the color change is an additional confirmation of the presence of negatively charged F4-TCNQ molecules. The latter (intermediate) state evolved when heating an extra 3 hours, after which the color changed from intense green to light green (Fig. 3A(c)). In contrast to what one might expect, this was accompanied by the disappearance of the F4-TCNQ anion bands. Once this state was reached, extra heating did not change the color of the solution nor its corresponding UV-VIS spectrum: the F4-TCNQ/MEK solution was stabilized at its thermodynamically favorable state where F4-TCNQ was no longer negatively charged. This phenomenon was observed for every concentration in the range of 2.5 to

40 mg F4-TCNQ ml^{-1} MEK, when one keeps in mind that a higher concentration requires a longer heating and stirring time (i.e. for 40 mg F4-TCNQ ml^{-1} MEK, 12 hours is necessary). We note that the solubility terminology used here in fact is only employed to refer to the physical state where F4-TCNQ as a powder is dissolved in the solvent MEK. From a chemical point of view, a different species is being formed, as will be clarified further on in the paper.

The same heating and stirring procedure was performed for a solution of 20 mg F4-TCNQ ml^{-1} acetonitrile. The bands corresponding to F4-TCNQ radical anions were also present in the UV-VIS spectrum. In contrast with F4-TCNQ in MEK, the bands did not disappear in time upon heating and stirring and no color change to green was observed (see Fig. 3B). This reveals a different interaction of F4-TCNQ with MEK as compared to that with acetonitrile.

2.1.2 Layer formation through spin coating of F4-TCNQ/ MEK solutions and layer characterization. In a next step we studied the solvent-assisted deposition of F4-TCNQ. To deposit a thin coating of F4-TCNQ molecules on a substrate, we applied
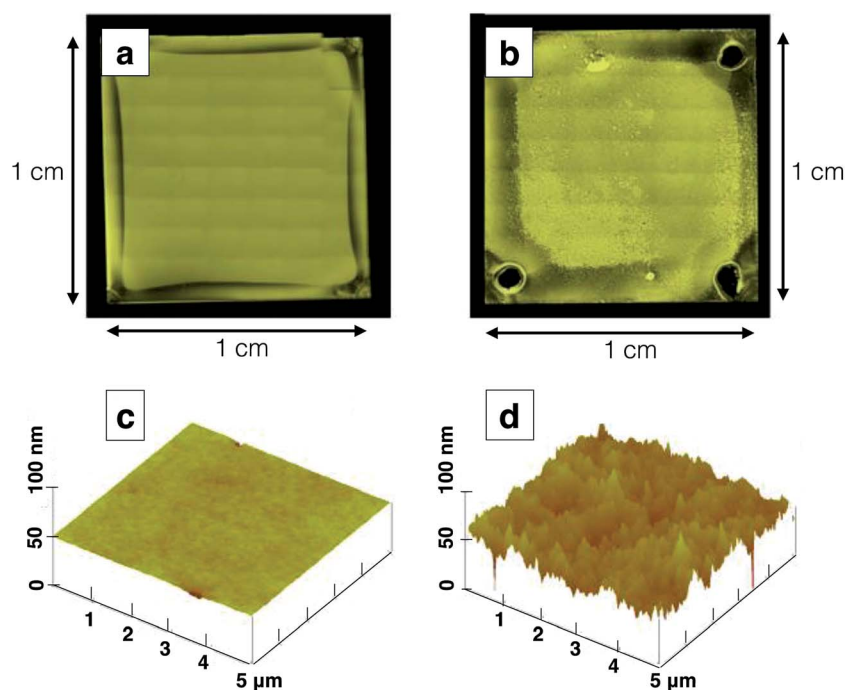
Fig. 5 Microscopy images of (a) the F4-TCNQ/MEK layer and (b) the F4-TCNQ/acetonitrile deposition after spin coating the solutions. The small squares observed in the pictures result from the stitching of the separate microscope images. Nomarski contrast is used to enhance the visual image. The pictures (c) and (d) are 3D surface plots taken by AFM of the F4-TCNQ/MEK layer and the F4-TCNQ/acetonitrile deposition, respectively, to show solvent related differences in roughness.

spin coating of the dopant solution and used silicon (Si) samples (1 × 1 cm) as substrate with a polished top side exhibiting a very high surface quality (RMS roughness of only 0.5 nm/25 μm²). This excellent surface quality of the substrate enabled us to adequately characterize the surface properties of the deposited F4-TCNQ.

We first performed spin coating tests for a dopant solution of 20 mg F4-TCNQ ml^{-1} MEK. Once the solution was stabilized (*i.e.* after heating and stirring for 5 hours), we found that spin coating the F4-TCNQ/MEK solution yielded a solid and uniform layer with a smooth surface. This is due to the arrangement of the F4-TCNQ and the MEK solvent molecules in a homogeneous layer as illustrated in Fig. 5a. The obtained RMS value equals the one for the bare polished Si-substrates (0.5 nm/25 μm²). The deposited layer thus has a surface roughness that corresponds with an optical quality of λ/1000 at a wavelength of 500 nm over a surface of 25 μm².

In contrast, spin coating a solution of 20 mg F4-TCNQ ml^{-1} acetonitrile did not produce a homogeneous F4-TCNQ deposition. This is due to a complete solvent evaporation during the spin coating process as no specific solvent-F4-TCNQ interactions occur. As a result, F4-TCNQ clusters are visible on the substrate, as illustrated in Fig. 5b. The obtained RMS value is 14.6 nm/25 μm², which is approximately 30 times higher than the RMS value of 0.5 nm/25 μm² obtained for F4-TCNQ/MEK, the latter being solely due to the underlying Si substrate.

The reason why only MEK yields a smooth layer resides in its ketone function. To validate our hypothesis, we also tested several other ketone solvents for their solubility and layer formation capacities in combination with F4-TCNQ: acetone, cyclohexanone, pentan-3-one, 3-methyl-butan-2-one and 4-methyl-pentan-2-one (Fig. 4b–f). Each of them was found to exhibit a high solubility for F4-TCNQ (up to 100 mg ml^{-1}, comparable with MEK), and spin coating F4-TCNQ solutions with these ketone solvents also yielded layers with similarly low surface roughness (*i.e.* RMS values < 1 nm/25 μm²) as obtained with MEK, thus confirming that the ketone function is the crucial factor in the layer formation mechanism. We note that a layer is being formed for F4-TCNQ concentrations ranging from 1 mg to 100 mg ml^{-1} ketone solvent. Moreover, it is important to stipulate that the layer formation is independent of the type of substrate used (silicon and in a later phase glass or graphene).

The layer formation of F4-TCNQ in MEK and in ketones in general, is also beneficial for the uniformity of the applied coating. The uniformity was measured with XPS and Table 1 summarizes the results; the small standard deviation confirms the high uniformity of the spin coated solid layer. The presence of ±5% oxygen and a higher amount of carbon in the layer (compared to the surface composition of a bare Si sample (as a reference) and relative to the amount of fluorine and nitrogen) is originating from MEK, confirming the incorporation of MEK solvent molecules in the obtained dopant layer. The XPS results of the other F4-TCNQ/ketone layers show that also there the solvent molecules are present in the layer.

To fully assess the optical-quality aspect of the dopant layer, we also performed optical transmission measurements of a 170

Table 1 XPS results of a bare Si substrate and a spin coated F4-TCNQ/MEK layer on a Si substrate (concentration = 20 mg F4-TCNQ ml^{-1} MEK). The table summarizes the average values and the corresponding standard deviations derived from measurements at four randomly selected positions on the surface

Element	Bare Si-sample (reference)		Si-sample with F4-TCNQ/MEK layer	
	Average (%)	Std. dev. (%)	Average (%)	Std. dev. (%)
O	35.81	0.8	5.13	0.3
C	22.31	1.9	63.46	0.2
N			14.66	0.1
F			16.76	0.3
Si	41.88	1.1		

nm-thick F4-TCNQ/MEK layer spin coated on a glass substrate to analyze its optical transparency in more detail over the broad wavelength range from 550 nm to 1900 nm. Once the dopant solution was stabilized, the resulting spin coated layer did not diminish the transmittance over this entire wavelength range, as shown in Fig. 6. As such, the layer offers real transparency for wavelengths between 550 and 1900 nm. We note that the transmittance of the glass substrate with a spin coated F4-TCNQ/MEK layer is slightly higher compared to that of a bare glass substrate due to interference effects induced by the layer, as we also verified theoretically. We point out that we included the thickness of the spin coated F4-TCNQ/MEK layers for different concentrations F4-TCNQ in the ESI (Fig. S3†).

Thus, F4-TCNQ combined with MEK (and more generally ketones) proves to be a very promising dopant system for optical and photonic applications, resulting in a uniform, smooth and optically transparent layer. The high solubility of F4-TCNQ in MEK is also an important asset for its use as dopant solution (see Section 2.2). In the next section, we investigate the interactions between the F4-TCNQ and MEK molecules that are responsible for the observed layer formation.

2.1.3 Analysis of F4-TCNQ/MEK interactions using ^{19}F-NMR and ^{13}C-NMR spectroscopy. To further elucidate the interactions between F4-TCNQ and MEK (and other ketone solvents), liquid-state as well as solid-state NMR spectroscopy was performed. Fig. 7 presents the ^{19}F solid-state NMR spectrum of F4-TCNQ, showing two signals of equal intensity. Although at first sight a single signal would be expected considering the chemical structure of F4-TCNQ (Fig. 2), the two resonances in the solid-state spectrum can be attributed to the two asymmetric unit cells which F4-TCNQ is constructed of (inset of Fig. 7).

Subsequently, liquid-state ^{19}F-NMR spectra were acquired of solutions of F4-TCNQ in several ketone solvents, all showing two times a double peak, *i.e.* a combination of two different F4-TCNQ signals with approximately a 65/35 molar ratio as demonstrated for a F4-TCNQ/MEK solution in Fig. 8a. As shown by the ^{19}F COSY 2D spectrum in Fig. 9, it is clear that the large downfield (or small upfield) peaks represent fluorine spins which are J-coupled with each other. However, the fluorine
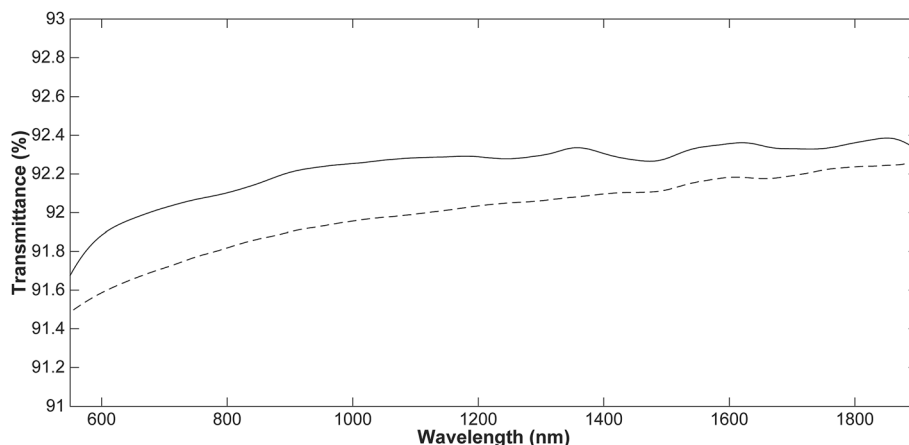
Fig. 6 Optical transmittance of a glass slide (grey dashed line) and a F4-TCNQ/MEK layer spin coated on glass (black full line).
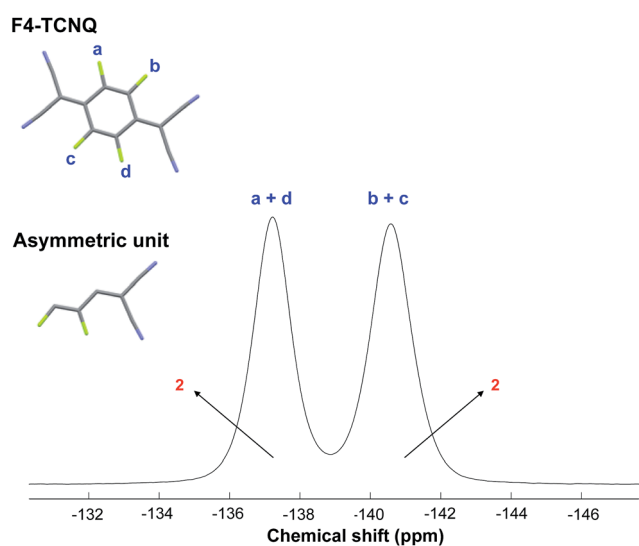

Fig. 7 ^{19}F solid-state NMR spectrum of F4-TCNQ. The two peaks in the spectrum are stemming from the two asymmetric unit cells which F4-TCNQ is constructed of (see inset with the nitrogen atoms represented by blue and fluorine atoms by green colors). The red labels in the spectrum show the relative integration values of the corresponding peaks.

Fig. 8 ^{19}F liquid-state NMR spectra of F4-TCNQ dissolved in (a) MEK and (b) acetonitrile. The red labels show the relative integration values of the corresponding peaks. The inset represents a F4-TCNQ molecule with nitrogen atoms indicated in blue and fluorine atoms indicated in green colors.

spins contributing to the large peaks are not J-coupled to those contributing to the small peaks, meaning that these fluorine spins belong to two different spin systems. This can only be explained by two fractions of F4-TCNQ molecules which interact with the ketone solvent along different configurations and one of which is dominant (involving 65% of the F4-TCNQ molecules). Since no averaged ^{19}F signal is observed in the NMR spectra, the rate of exchange between these two different configurations has to be slow compared to the NMR time scale (see below). Conversely, F4-TCNQ in acetonitrile (Fig. 8b) leads to one broad peak corresponding to all fluorine atoms. The reason why the two signal combinations (stemming from the contribution of the asymmetric unit cells) are not resolved can already be found in the UV-VIS spectra: since F4-TCNQ in

acetonitrile remains negatively ionized, the unpaired electron causes very fast (paramagnetic) T_2 relaxation and consequently severe line broadening (decreasing relaxation time (T_2) ∼ increasing relaxation rate ($1/T_2$) ∼ increasing width at half height ($\nu_{1/2}$)).[47]

These findings were also clearly confirmed by the presence of three MEK carbonyl signals in ^{13}C-NMR spectra (see Fig. S2 of ESI†): next to one signal around 207.2 ppm originating from

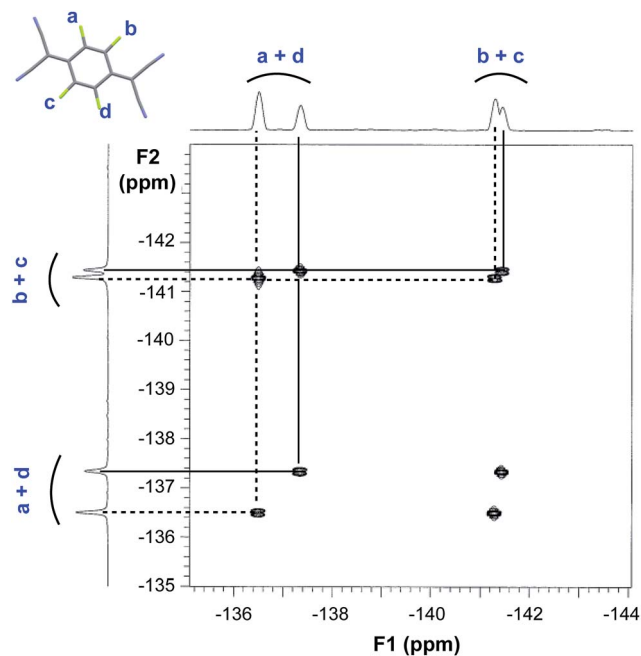Fig. 9 ¹⁹F COSY 2D spectrum of F4-TCNQ dissolved in MEK. The solid and dotted lines indicate the J-coupled peaks, corresponding to two different chemical environments for F4-TCNQ in MEK. The inset represents a F4-TCNQ molecule with nitrogen atoms indicated in blue and fluorine atoms indicated in green colors.

pure 'free' MEK, there exist two additional signals in a 65/35 ratio between 202–204 ppm which correspond to MEK that is 'bounded' to F4-TCNQ along two different geometries. Based on the frequency difference between the signals of 'free' and 'bounded' MEK (roughly 4 ppm, i.e. 400 Hz), the rate of exchange between free and bounded MEK has to be smaller than 400 Hz and hence relatively slow. Since no additional solvent peaks are observed in the ¹³C-NMR spectrum of F4-TCNQ in acetonitrile (see Fig. S1b of ESI†), we can thus assume that no stable interactions take place between F4-TCNQ and acetonitrile.

The NMR experiments confirm the presumption that F4-TCNQ molecules dissolved in MEK (or ketone solvents)

strongly interact with MEK, resulting in slower solvent evaporation during spin coating so that the F4-TCNQ and solvent molecules can form a self-assembled layer after spin coating.

Further details on the results obtained through ¹³C-NMR spectroscopy can be found in the ESI.†

2.1.4 Analysis of F4-TCNQ/MEK interactions through quantum chemical calculations. A theoretical understanding of the above described observations is given by quantum chemical calculations. The results of the calculations are presented in Table 2. Non-ketone solvents, such as chloroform and acetonitrile, bind less strongly to F4-TCNQ (the gas-phase B3LYP + BSSE calculations indicate smaller interaction energies in absolute values for these solvents as compared to ketone solvents), which is consistent with their poor solubility or incapacity to form layers with the dopant molecule, respectively. Also the enol form of acetone (after undergoing keto–enol tautomery) does not reveal favourable binding properties. The values of the interaction energy, after the inclusion of dispersive interactions in the description of the energy (see gas-phase ωB97XD + BSSE calculations vs. gas-phase B3LYP + BSSE calculations), dramatically increase in absolute value, slightly altering the ratios between them, and they still show less interaction for the solvents mentioned above than for ketones. In the gas phase the electron charge transfer (q for ωB97XD + BSSE) appears to occur from F4-TCNQ towards the ketone MEK, so that the ketone unexpectedly serves as acceptor for F4-TCNQ electrons while acetonitrile acts as donor. We see the same trend in the solvent phase (see ωB97XD + PCM calculations) for both the MEK and cyclohexanone ketone solvents. These findings are in agreement with the UV-VIS spectra recorded for the F4-TCNQ/MEK solution; in the thermodynamically stabilized phase, the anion peaks were no longer present (Fig. 3A(c)). The calculations suggest that there is only a small contribution to the overall stabilization from the charge transfer between the molecules, which is generally enhanced by the use of a solvent-continuum, as expected, and that the largest part of the stabilization is due to dipolar interactions and dispersion, considering the large increase in stabilization energy when the dispersion contribution to the total energy is included in ωB97XD. In the case of MEK, a small fraction of electronic

Table 2 Interaction energies E (in kJ mol⁻¹) and the resulting charge q (in a.u.) on the F4-TCNQ fragment of the one-to-one complexes of F4-TCNQ combined with 6 different solvent molecules employed, as calculated using B3LYP, ωB97XD and ωB97XD + PCM, with BSSE and PCM (calculated with dielectric constant for MEK $\varepsilon = 18.246$, cyclohexanone $\varepsilon = 15.619$, acetone $\varepsilon = 20.493$, acetonitrile $\varepsilon = 35.688$ and chloroform $\varepsilon = 4.711$, see text for details)

	B3LYP + BSSE	ωB97XD + BSSE	ωB97XD + BSSE	ωB97XD	ωB97XD + PCM	ωB97XD + PCM
	E	E	q	E	E	q
MEK	−22.65	−45.71	0.001	−52.34	−32.17	0.015
Cyclohexanone	−24.07	−39.43	−0.021	−45.15	−32.63	0.022
Acetone	−23.36	−38.97	−0.021	−44.58	−23.83	−0.026
Acetone (enol)	−14.19	−18.29	0.061	−20.13	−17.20	0.073
Acetonitrile	−22.40	−35.29	−0.014	−39.26	−17.28	−0.011
Chloroform	−2.60	−28.72	−0.090	−40.08	−33.73	−0.094

charge ($q = 0.015$ for ωB97XD + PCM) is transferred from F4-TCNQ as donor to the ketone solvent as acceptor molecule in their thermodynamically stable state, and a strongly negative interaction energy of -31.52 kJ mol^{-1} is found for F4-TCNQ in MEK (ωB97XD + PCM). The extra-ordinary behavior of F4-TCNQ as donor when dissolved in MEK indicates a pre-organization of the molecules already in the solution phase, comprising two specific intermolecular configurations as found in Section 2.1.3, and yields a uniform layer incorporating both F4-TCNQ and solvent molecules after spin coating. We can therefore assume that the ketone solvent molecules act as a "linker" between F4-TCNQ molecules in the smooth, uniform layer.

2.2 Doping of graphene with an F4-TCNQ/MEK layer

The previous sections clearly reveal the advantageous chemical and optical properties of F4-TCNQ in MEK (or ketones in general). Indeed, a uniform and optically transparent layer can be formed for a wide range of F4-TCNQ concentrations. In the second part of the paper, we present the details about the actual doping effect on graphene and discuss the ability to control the doping effect by varying the F4-TCNQ concentration.

We performed doping experiments on two types of graphene: on the one hand p-type hydrogen-intercalated quasi-free-standing monolayer graphene grown on 6H-silicon-carbide (SiC) (0001) substrates and on the other hand monolayer graphene provided by CVD growth on copper and electrochemically transferred onto Si substrates. The doping was monitored and quantified *via* Hall effect measurements, an effective way to measure the electrical parameters of graphene.

2.2.1 Doping of graphene grown on SiC substrates. In a first stage, we focused on epitaxial hydrogen-intercalated quasi-free-standing graphene grown on SiC substrates because it is known that this type of graphene consistently exhibits high quality:[48] graphene grown on 6H-SiC (0001) features p-type doping in the range between $n = +8.5 \times 10^{12}$ cm^{-2} and $+1.5 \times 10^{13}$ cm^{-2}, and a mobility μ up to 3000 cm^2 V^{-1} s^{-1}. After doping graphene with the electron-acceptor F4-TCNQ, an increase of the p-type charge carrier concentration and as a consequence a decrease of the sheet resistance is expected. The mobility of graphene will decrease unavoidably after doping, but we aim at keeping the mobility as high as possible.[49] In Fig. 10A and Table S1† the experimental results of the Hall measurements before and after doping graphene on 6H-SiC substrates with a F4-TCNQ/MEK layer are shown for dopant concentrations ranging from 2.5 to 40 mg ml^{-1}.

Regardless the F4-TCNQ concentration applied, an increase in charge carrier concentration was consistently observed together with a reduction of the sheet resistance, as anticipated. Despite the significant increase in charge carrier concentrations, the mobility decreased less than 50% and remained high ($\mu > 1000$ cm^2 V^{-1} s^{-1}).

The change in charge carrier concentration as a function of the F4-TCNQ concentration (Fig. 10A) exhibits a clear trend. Indeed, in the first region of the F4-TCNQ concentration range, *i.e.* from 2.5 to 7.5 mg F4-TCNQ ml^{-1} MEK, we notice a strongly increasing doping effect with increasing dopant concentration.
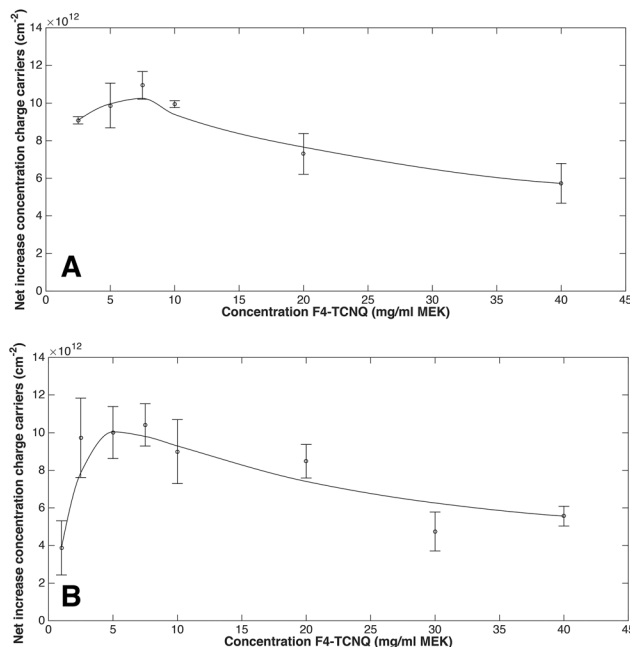

Fig. 10   Fitted curve for the change in charge carrier concentration (Δn in cm^{-2}) after doping of (A) epitaxial graphene (quasi-free-standing on SiC substrates (6H)) and (B) CVD grown graphene on copper and transferred to Si substrates with an F4-TCNQ/MEK layer as a function of the concentration of F4-TCNQ. Each dopant solution is applied to three different samples, and the curve is fitted along the moving average method (window size = 3).

The maximal doping effect of $\Delta n = +1.09 \times 10^{13}$ cm^{-2} (on the curve fitted along the moving average method) was reached at 7.5 mg F4-TCNQ ml^{-1} MEK, corresponding with a decrease of the Fermi level of 0.20 eV and a 40% decrease of the sheet resistance. This increase in doping effect is in line with the literature on graphene doping with F4-TCNQ,[35,50,51] and with other dopant molecules:[52,53] generally, the deposition of more electron withdrawing molecules on graphene will enhance the electron transfer from graphene, resulting in a stronger doping effect. In the second region of the F4-TCNQ concentration range, *i.e.* above 7.5 mg ml^{-1} MEK, a decreasing doping effect is observed with increasing dopant concentration, being indicative for saturation. Several factors are contributing to this saturation effect: a higher F4-TCNQ concentration leads to a denser F4-TCNQ distribution at the graphene interface, which yields increasing intermolecular repulsion forces between charged F4-TCNQ molecules[51] and an increasing capturing probability for freely moving holes of graphene due to the presence of more ionized attraction centers.[54] Due to this saturation mechanism, increasing the F4-TCNQ concentrations will only give rise to relatively more neutral F4-TCNQ molecules, which will not contribute to the electron uptake.[55] The best compromise between the F4-TCNQ-MEK molecular organization at the graphene interface and the doping capacities of F4-TCNQ, is reached at a concentration of 7.5 mg F4-TCNQ ml^{-1} MEK. Given this concentration dependence, we can control the net increase in doping of graphene over the range from $\Delta n = +5.73 \times 10^{12}$ cm^{-2} to $+1.09 \times 10^{13}$ cm^{-2}.

We note that these results were obtained about 10 days after the doping was applied. Because the organic doping layer consists of connected F4-TCNQ molecules with the ability to strongly delocalize the electrons, the values were slowly changing during the first days until stabilization was obtained. Once the maximal doping effect was reached, it remained constant (a maximum change of 10% of the doping value is observed), over a period of several months when preserving the samples at room temperature, in a dark and humid free environment.

2.2.2 Doping of graphene transferred onto Si substrates. In order to verify whether our doping procedure is affected by the type of graphene or the substrate, the same experiments and dopant solutions were applied to graphene provided by CVD growth on copper and electrochemically transferred on Si samples. When aiming at implementing graphene in optical or electronic applications, transferring graphene on a freely chosen substrate is necessary. Typical Hall characterization results[56] for this type of graphene indicate a p-type charge carrier concentration n of the order of $+(2-6) \times 10^{12}$ cm^{-2}, a mobility μ ranging from 300 to 2000 cm^2 V^{-1} s^{-1} and a sheet resistance R in the range of 1.2–2.6 kΩ sq^{-1}. The values before and after applying the dopant solution F4-TCNQ/MEK are presented in Fig. 10B and Table S2.†

Keeping in mind the above mentioned typical values for the initial electrical parameters of CVD-grown transferred graphene,[56] we made a selection of our samples such that all of them fulfilled the conditions of a high mobility ($\mu > 700$ cm^2 V^{-1} s^{-1}) and low sheet resistance ($R < 2$ kΩ sq^{-1}), as ultimate quality validation.

We find that the maximum net doping effect is reached at the concentration of 7.5 mg F4-TNCQ ml^{-1} MEK, as observed before for graphene on SiC substrates, and the maximum doping effect is of the same order of magnitude as the maximum found previously (Δn around $+1.0 \times 10^{13}$ cm^{-2}, corresponding with a decrease of 0.21 eV in Fermi energy and a 41% decrease of the sheet resistance), although the two types of graphene are quite different and the CVD graphene features a lower mobility (on average $\mu_{\text{6H-SiC}}$ (2500 cm^2 V^{-1} s^{-1}) > μ_{CVD} (1500 cm^2 V^{-1} s^{-1})). Since the increasing doping trend for dopant concentrations from 2.5 to 7.5 mg F4-TCNQ ml^{-1} MEK was less pronounced here than it was for graphene on SiC substrates, we included an extra concentration below 2.5 mg (*i.e.* 1 mg F4-TCNQ ml^{-1} MEK) to verify this trend. When applying again the moving average method for fitting the curve in Fig. 10B, we observe the same trend as for graphene on SiC substrates. Also here a saturation regime with lowering doping effect is present for concentrations higher than 7.5 mg F4-TCNQ ml^{-1} MEK.

The doping effect on graphene can also be expressed in terms of change in sheet conductance ($\Delta\sigma$ [mS]); the same trend is observed as noticed for the change in charge carrier concentration (Fig. S4 in ESI†). To complete the analysis of the doping effect, we also performed Raman spectroscopy measurements on graphene before and after doping. These measurements clearly show a frequency-upshifting of the 2D-band and G-band, being indicative for p-type doping (Fig. S5 in ESI†).

Since other ketone solvents also feature similar benefits regarding solubility and layer formation for F4-TCNQ doping, a preliminary study about the doping effect of F4-TCNQ dissolved in other ketone solvents was also performed. We could establish a structure–activity relation. Indeed, the larger the solvent molecule, the higher the F4-TCNQ concentration required to reach the maximum doping effect. This observation originates from the molecular organization in the layer; since the ketone molecules are incorporated in the dopant layer, using larger solvent molecules yields a lower density of F4-TCNQ molecules in the layer as compared to their density in an F4-TCNQ/MEK layer. Therefore, there is less direct contact between graphene and F4-TCNQ in case larger ketone molecules than MEK are used. Acetone is the only ketone molecule that is smaller than MEK, but there the layer formation encounters difficulties due to acetone's higher susceptibility to water and lower boiling point in comparison with MEK. Consequently, MEK will be the most promising solvent as it embodies stable layer formation and yields the maximum doping effect at the lowest F4-TCNQ concentration compared to the other ketone solvents. A comprehensive ketone solvent study for F4-TCNQ doping will be published in a separate paper.

2.2.3 Comparison between doping of graphene with F4-TCNQ evaporated powder and with F4-TCNQ/MEK layer. We mentioned earlier the research of Coletti *et al.*,[35] where F4-TCNQ doping was applied to obtain charge neutrality of initially n-doped graphene. They deposited F4-TCNQ on graphene *via* thermal evaporation in ultrahigh vacuum, resulting in a powder-like coating. The obtained change in charge carrier concentration after full coverage with F4-TCNQ was reported to be $+7.15 \times 10^{12}$ cm^{-2}. The latter value is significantly smaller than the doping capacity obtained here for the F4-TCNQ/MEK layer at the optimal concentration of 7.5 mg F4-TCNQ ml^{-1} MEK, namely $\Delta n = +1.09 \times 10^{13}$ cm^{-2} for epitaxial hydrogen-intercalated graphene on SiC substrates and $\Delta n = +1.05 \times 10^{13}$ cm^{-2} for graphene transferred from copper on Si samples (see Fig. 10A and B).

Hence, when F4-TCNQ is organized in a layer together with the MEK solvent, the electron withdrawing activity at the graphene interface is approximately 50% stronger than when F4-TCNQ is deposited as a powder on graphene. The reasons underpinning this finding are twofold. A first reason was already given in the previous section on the quantum chemical calculations for the interactions between F4-TCNQ and MEK as a charge transfer complex. Table 2 showed for the ωB97XD + PCM calculations that the resulting charge q on the F4-TCNQ fragment for the one-to-one complex equals $+0.015$ (in a.u.), indicating that the overall electron withdrawing capacities for F4-TCNQ dissolved in MEK will be stronger. The second reason can be traced back to the spatial organization of the layer. The incorporated MEK solvent molecules are surrounding the F4-TCNQ molecules in the layer as "linker" molecules, hence reducing the repulsion between charged F4-TCNQ molecules and facilitating the charge delocalization through the organization of a connected F4-TCNQ "chain" in the organic layer. Hence the MEK solvent molecules will enhance the electron transfer between graphene and F4-TCNQ.

As pointed out in the introduction, apart from our F4-TCNQ based graphene doping method, also other techniques have been reported where very high transparency of the dopant system has been achieved over a given wavelength domain, and one of them, namely the plasma treatment-based method of Pham et al.,[15] even achieved a 60% reduction of the sheet resistance of CVD graphene, while the corresponding reduction in this paper equals 41%. However, as opposed to the method of Pham et al., our doping approach offers for the first time both very high transparency and a very low surface roughness, the latter being extremely important to avoid light scattering in optical applications. Furthermore, the herein proposed method does not require ultrahigh vacuum or plasma treatment and is very practical from a technological point of view, hence generally enhancing the applicability of F4-TCNQ-based graphene doping through wet chemistry approaches. These properties enable for the first time controllable chemical graphene doping with true optical quality as required for optical and photonic applications and components such as photonic integrated devices and nonlinear wavelength converters.

3. Conclusion

We have developed a new controllable chemical doping method for graphene fulfilling for the first time the requirement of optical transparency and low surface roughness as needed for optical and photonic applications. This method relies on combining the electron-acceptor F4-TCNQ with ketone solvents such as MEK. Ketones exhibit an excellent solubility for F4-TCNQ over a wide dopant concentration range. When spin coating the F4-TCNQ/MEK solution, a uniform homogeneous layer is formed, regardless the type of substrate used (silicon, glass or graphene). Moreover, the F4-TCNQ/MEK layer exhibits a very low surface roughness corresponding to an optical quality of λ/1000 (at the wavelength of 500 nm) when spin coated on polished Si samples and is highly transparent over a wide wavelength range from 550 to 1900 nm. The layer formation mechanism relies on the ketone functional group that engages in a specific interaction with the F4-TCNQ molecules based on an extra-ordinary charge transfer complex.

Through Hall measurements, we have found that the F4-TCNQ/MEK layers induce effective p-doping for initially (weakly) p-type graphene: the charge carrier concentration increases significantly while still enabling high carrier mobility in the graphene sheet. The doping effect is controllable with a net increase in charge carrier concentration ranging from $\Delta n = +5.73 \times 10^{12}$ cm^{-2} to $+1.09 \times 10^{13}$ cm^{-2} (for epitaxial hydrogen-intercalated graphene (6H) on SiC substrates) or from $\Delta n = +5.56 \times 10^{12}$ cm^{-2} to $+1.04 \times 10^{13}$ cm^{-2} (for graphene transferred from copper to Si samples) when varying the dopant concentrations from 2.5 to 40 mg F4-TCNQ ml^{-1} MEK. These values show that F4-TCNQ incorporated in a layer exhibits an up to 50% higher doping efficiency in comparison with thermally evaporated F4-TCNQ on epitaxial graphene on SiC.

Together with the beneficial layer uniformity, smoothness and optical transparency, this new chemical doping approach is most viable in particular when optical-quality graphene doping for optical and photonic applications is required.

Acknowledgements

References

1 F. Bonaccorso, Z. Sun, T. Hasan and A. Ferrari, *Nat. Photonics*, 2010, **4**, 611–622.

2 A. Balandin, S. Ghosh, W. Bao, I. Calizo, D. Teweldebrhan, F. Miao and C. N. Lau, *Nano Lett.*, 2008, **8**, 902–907.

3 J. Moser, A. Barreiro and A. Bachtold, *Appl. Phys. Lett.*, 2007, **91**, 4–6.

4 S. V. Morozov, K. S. Novoselov, M. I. Katsnelson, F. Schedin, D. C. Elias, J. A. Jaszczak and A. K. Geim, *Phys. Rev. Lett.*, 2008, **100**, 16602.

5 C. Lee, X. Wei, J. W. Kysar and J. Hone, *Science*, 2008, **321**, 385–388.

6 K. F. Mak, L. Ju, F. Wang and T. F. Heinz, *Solid State Commun.*, 2012, **152**, 1341–1349.

7 I. Gierz, C. Riedl, U. Starke, C. R. Ast and K. Kern, *Nano Lett.*, 2008, **8**, 4603–4607.

8 Y.-J. Yu, Y. Zhao, S. Ryu, L. E. Brus, K. S. Kim and P. Kim, *Nano Lett.*, 2009, **9**, 3430–3434.

9 H. Liu, Y. Liu and D. Zhu, *J. Mater. Chem.*, 2011, **21**, 3335.

10 P. Rani and V. K. Jindal, *RSC Adv.*, 2013, **3**, 802–812.

11 Z.-H. Sheng, H.-L. Gao, W.-J. Bao, F.-B. Wang and X.-H. Xia, *J. Mater. Chem.*, 2012, **22**, 390–395.

12 Y. Shao, S. Zhang, M. H. Engelhard, G. Li, G. Shao, Y. Wang, J. Liu, I. A. Aksay and Y. Lin, *J. Mater. Chem.*, 2010, **20**, 7491–7496.

13 H. Pinto, R. Jones, J. P. Goss and P. R. Briddon, *Phys. Status Solidi B*, 2010, **207**, 2131–2136.

14 T. Hu and I. C. Gerber, *J. Phys. Chem. C*, 2013, **117**, 2411–2420.

15 V. P. Pham, K. H. Kim, M. H. Jeon, S. H. Lee, K. N. Kim and G. Y. Yeom, *Carbon*, 2015, **95**, 664–671.

16 R. R. Nair, A. N. Grigorenko, P. Blake, K. S. Novoselov, T. J. Booth, N. M. R. Peres, T. Stauber and A. K. Geim, *Science*, 2008, **320**, 1308.

17 P. Blake, P. D. Brimicombe, R. R. Nair, T. J. Booth, D. Jiang, F. Schedin, L. A. Ponomarenko, S. V. Morozov, H. F. Gleeson, E. W. Hill, A. K. Geim and K. S. Novoselov, *Nano Lett.*, 2008, **8**, 1704–1708.

18 X. Li, C. W. Magnuson, A. Venugopal, J. An, J. W. Suk, B. Han, M. Borysiak, W. Cai, A. Velamakanni, Y. Zhu, L. Fu, E. M. Vogel, E. Voelkl, L. Colombo and R. S. Ruoff, *Nano Lett.*, 2010, **10**, 4328–4334.

19 S. H. Kim, W. Song, M. W. Jung, M. A. Kang, K. Kim, S. J. Chang, S. S. Lee, J. Lim, J. Hwang, S. Myung and K. S. An, *Adv. Mater.*, 2014, **26**, 4247–4252.

20 D. Choi, C. Kuru, C. Choi, K. Noh, S. Hwang, W. Choi and S. Jin, *Small*, 2015, 3143–3152.

21 F. Güneş, H. J. Shin, C. Biswas, G. H. Han, E. S. Kim, S. J. Chae, J. Y. Choi and Y. H. Lee, *ACS Nano*, 2010, **4**, 4595–4600.

22 J. Wu, L. Xie, Y. Li, H. Wang, Y. Ouyang, J. Guo and H. Dai, *J. Am. Chem. Soc.*, 2011, **133**, 19668–19671.

23 A. Poruba, A. Fejfar, Z. Remeš, J. Špringer, M. Vaněček, J. Kočka, J. Meier, P. Torres and A. Shah, *J. Appl. Phys.*, 2000, **88**, 148–160.

24 M.-S. Dong, X.-M. Wu, Y.-L. Hua, Q.-J. Qi and S.-G. Yin, *Chin. Phys. Lett.*, 2010, **27**, 127802.

25 G. Lu, J. Blakesley, S. Himmelberger, P. Pingel, J. Frisch, I. Lieberwirth, I. Salzmann, M. Oehzelt, R. Di Pietro, A. Salleo, N. Koch and D. Neher, *Nat. Commun.*, 2013, **4**, 1588.

26 W. Chen, D. Qi, X. Gao and A. T. S. Wee, *Prog. Surf. Sci.*, 2009, **84**, 279–321.

27 T. Takenobu, T. Kanbara, N. Akima, T. Takahashi, M. Shiraishi, K. Tsukagoshi, H. Kataura, Y. Aoyagi and Y. Iwasa, *Adv. Mater.*, 2005, **17**, 2430–2434.

28 L. Cosimbescu, A. B. Padmaperuma and D. J. Gaspar, *J. Phys. Chem. A*, 2011, **115**, 13498–13503.

29 L. R. Melby, R. J. Harder, W. R. Hertler, W. Mahler, R. E. Benson and W. E. Mochel, *J. Am. Chem. Soc.*, 1962, **84**, 3374–3387.

30 H. Pinto, R. Jones, J. P. Goss and P. R. Briddon, *J. Phys.: Condens. Matter*, 2009, **21**, 402001.

31 M. Rudloff, K. Ackermann, M. Huth, H. O. Jeschke, M. Tomic, R. Valentí, B. Wolfram, M. Bröring, M. Bolte, D. Chercka, M. Baumgarten and K. Müllen, *Phys. Chem. Chem. Phys.*, 2015, **17**, 4118–4126.

32 S. J. Sque, R. Jones and P. R. Briddon, *Phys. Status Solidi B*, 2007, **204**, 3078–3084.

33 T. Kuila, S. Bose, A. K. Mishra, P. Khanra, N. H. Kim and J. H. Lee, *Prog. Mater. Sci.*, 2012, **57**, 1061–1105.

34 V. Georgakilas, M. Otyepka, A. B. Bourlinos, V. Chandra, N. Kim, K. C. Kemp, P. Hobza, R. Zboril and K. S. Kim, *Chem. Rev.*, 2012, **112**, 6156–6214.

35 C. Coletti, C. Riedl, D. S. Lee, B. Krauss, L. Patthey, K. von Klitzing, J. H. Smet and U. Starke, *Phys. Rev. B: Condens. Matter Mater. Phys.*, 2010, **81**, 235401.

36 W. Chen, S. Chen, D. C. Qi, X. Y. Gao, A. Thye and S. Wee, *J. Am. Chem. Soc.*, 2007, **129**, 10418–10422.

37 C.-L. Hsu, C.-T. Lin, J.-H. Huang, C.-W. Chu, K.-H. Wei and L.-J. Li, *ACS Nano*, 2012, **6**, 5031–5039.

38 K.-H. Yim, G. L. Whiting, C. E. Murphy, J. J. M. Halls, J. H. Burroughes, R. H. Friend and J.-S. Kim, *Adv. Mater.*, 2008, **20**, 3319–3324.

39 Y. Zhang, B. de Boer and P. W. M. Blom, *Adv. Funct. Mater.*, 2009, **19**, 1901–1905.

40 R. Matsunaga, K. Matsuda and Y. Kanemitsu, *Phys. Rev. Lett.*, 2011, **106**, 37404.

41 L. Ma, W. H. Lee, Y. D. Park, J. S. Kim, H. S. Lee and K. Cho, *Appl. Phys. Lett.*, 2008, **92**, 63310.

42 Y. Zhang and P. W. M. Blom, *Org. Electron.*, 2010, **11**, 1261–1267.

43 Y. Nosho, Y. Ohno, S. Kishimoto and T. Mizutani, *Nanotechnology*, 2007, **18**, 415202.

44 J. Brandrup, *Polymer Handbook*, 1999.

45 A. Jain, K. V. Rao, U. Mogera, A. A. Sagade and S. J. George, *Chem.–Eur. J.*, 2011, **17**, 12355–12361.

46 A. P. O'Mullane, N. Fay, A. Nafady and A. M. Bond, *J. Am. Chem. Soc.*, 2007, **129**, 2066–2073.

47 J. K. M. Sanders and B. K. Hunter, *Modern NMR spectroscopy: a guide for chemists*, Oxford University Press, 1987.

48 T. Ciuk and W. Strupinski, *Carbon*, 2015, **93**, 1042–1049.

49 L. Chen, L. Wang, Z. Shuai and D. Beljonne, *J. Phys. Chem. Lett.*, 2013, **4**, 2158–2165.

50 J. T. Sun, Y. H. Lu, W. Chen, Y. P. Feng and A. T. S. Wee, *Phys. Rev. B: Condens. Matter Mater. Phys.*, 2010, **81**, 155403.

51 X. Tian, J. Xu and X. Wang, *J. Phys. Chem. B*, 2010, **114**, 11377–11381.

52 Z. Chen, I. Santoso, R. Wang, L. F. Xie, H. Y. Mao, H. Huang, Y. Z. Wang, X. Y. Gao, Z. K. Chen, D. Ma, A. T. S. Wee and W. Chen, *Appl. Phys. Lett.*, 2010, **96**, 213104.

53 S. A. Paniagua, J. Baltazar, H. Sojoudi, S. K. Mohapatra, S. Zhang, C. L. Henderson, S. Graham, S. Barlow and S. R. Marder, *Mater. Horiz.*, 2014, **1**, 111–115.

54 M. L. Tietze, L. Burtone, M. Riede, B. Lüssem and K. Leo, *Phys. Rev. B: Condens. Matter Mater. Phys.*, 2012, **86**, 35320.

55 C. Wang and Y. Gao, *Appl. Phys. Lett.*, 2014, **105**, 111601.

56 T. Ciuk, I. Pasternak, A. Krajewska, J. Sobieski, P. Caban, J. Szmidt and W. Strupinski, *J. Phys. Chem. C*, 2013, **117**, 20833–20837.